Investigation into the effect on structure of oxoanion doping in $Na_2M(SO_4)_2 \cdot 2H_2O$

Driscoll, Laura; Wright, Adrian; Kendrick, Emma; Slater, Peter

DOI:
10.1016/j.jssc.2016.07.004

Document Version
Peer reviewed version

Citation for published version (Harvard):
Driscoll, L, Wright, A, Kendrick, E & Slater, P 2016, 'Investigation into the effect on structure of oxoanion doping in $Na_2M(SO_4)_2 \cdot 2H_2O$', *Journal of Solid State Chemistry*, vol. 242, no. Part 1, pp. 103-111. https://doi.org/10.1016/j.jssc.2016.07.004

Investigation into the effect on structure of oxoanion doping in $Na_2M(SO_4)_2 \cdot 2H_2O$

L.L. Driscoll, E. Kendrick, A.J. Wright, P.R. Slater

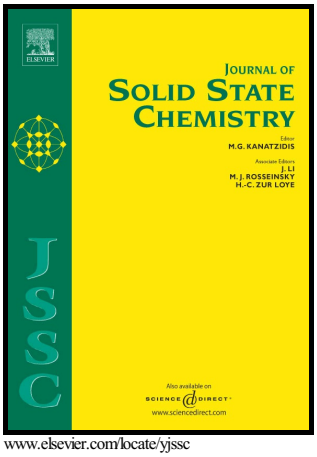

www.elsevier.com/locate/yjssc

PII: S0022-4596(16)30255-9
DOI: http://dx.doi.org/10.1016/j.jssc.2016.07.004
Reference: YJSSC19451

To appear in: *Journal of Solid State Chemistry*

Received date: 31 March 2016
Revised date: 8 June 2016
Accepted date: 4 July 2016

Cite this article as: L.L. Driscoll, E. Kendrick, A.J. Wright and P.R. Slater, Investigation into the effect on structure of oxoanion doping i $Na_2M(SO_4)_2 \cdot 2H_2O$, *Journal of Solid State Chemistry* http://dx.doi.org/10.1016/j.jssc.2016.07.004

Investigation into the effect on structure of oxoanion doping in $Na_2M(SO_4)_2 \cdot 2H_2O$

L.L. Driscoll[1], E. Kendrick[1,2], A. J. Wright[1] and P.R. Slater[1*]

1) School of Chemistry, University of Birmingham, Edgbaston, Birmingham, West Midlands B15 2TT
2) Sharp Laboratories Europe, Oxford Science Park, Edmund Halley Road, Oxford OX4 4GB

Correspondence to:

Prof. P.R. Slater

School of Chemistry, University of Birmingham, Edgbaston, Birmingham, West Midlands B15 2TT

p.r.slater@bham.ac.uk

Abstract

In this paper an investigation into the effect of transition metal ion and selenate/fluorophosphate doping on the structures of $Na_2M(SO_4)_2 \cdot 2H_2O$ (M=transition metal) materials is reported. In agreement with previous reports, the monoclinic (Kröhnkite) structure is adopted for M=Mn, Fe, Co, Cu, while for the smallest first row divalent transition metal ion, M=Ni, the triclinic (Fairfieldite structure) is adopted. On selenate doping there is a changeover in structure from monoclinic to triclinic, with the larger Mn^{2+} system requiring the highest level of selenate to complete the changeover. Thus the results suggest that the relative stability of the two structure types is influenced by the relative size of the transition metal: oxoanion group, with the triclinic structure favoured for small transition metals/large oxoanions.

The successful synthesis of fluorophosphate doped samples, $Na_2M(SO_4)_{2-x}(PO_3F)_x \cdot 2H_2O$ was also obtained for M=Fe, Co, Cu, with the results showing a changeover in structure from monoclinic to triclinic for M=Co, Cu for very low levels (x=0.1) of fluorophosphate. In the case of M=Fe, the successful synthesis of fluorophosphates samples was achieved for $x \leq 0.3$, although no change in cell symmetry was observed. Rather in this particular case, the X-ray diffraction patterns showed evidence for selective peak broadening, attributed to local disorder as a result of the fluorophosphate group disrupting the H-bonding network. Overall the work highlights how isovalent doping can be exploited to alter the structures of $Na_2M(SO_4)_2 \cdot 2H_2O$ systems.

Keywords: Sodium ion, Sulfate, Selenate, Fluorophosphate, Crystal Structure

1. Introduction

Minerals constructed from metal octahedra and oxoanion tetrahedra have a variety of applications including as battery electrodes [1–7], fuel cell materials [8–13], medical applications [14],[15] and pigments[16]. Many such mineral systems are hydrated, and in such systems hydrogen bonding also contributes to the bonding between the octahedral and tetrahedral units. One system that has attracted recent interest is $Na_2Fe(SO_4)_2 \cdot 2H_2O$ which has been investigated as a potential electrode material for Na ion batteries[2]. This material adopts the Kröhnkite structure (monoclinic cell), named after the mineral of that name, $Na_2Cu(SO_4)_2 \cdot 2H_2O$. The Kröhnkite structure is also adopted by $Na_2Mn(SO_4)_2 \cdot 2H_2O$ and $Na_2Co(SO_4)_2 \cdot 2H_2O$ [17] . In contrast, the equivalent Ni based system, $Na_2Ni(SO_4)_2 \cdot 2H_2O$, adopts the Fairfieldite structure (triclinic cell: named after the respective mineral, Fairfieldite: $Ca_2(Mn, Fe)(PO_4)_2 \cdot 2H_2O$). The sulfate group can be replaced by selenate in the

above systems, and the resultant $Na_2M(SeO_4)_2 \cdot 2H_2O$ (M=Co, Ni) systems have been reported to also adopt the Fairfieldite structure[18].

The structures of both consist of 3-dimensional networks composed of metal octahedra corner sharing with sulfate/selenate tetrahedra, with chains of $M(S/SeO_4)_4(H_2O)_2$ along the c-axis and the space between these chains occupied by the sodium ions (Fig. 1). Additional stabilisation results from the hydrogen bond network which creates a pseudo-layered structure. A key difference between the two structures is in terms of the H bonding network that links the layers: in the monoclinic Kröhnkite structure, two oxygen atoms in the sulfate tetrahedra participate in the network, while in the triclinic Fairfieldite structure, only 1 of the oxygen atoms in the tetrahedral unit is involved in the hydrogen bond network. This change also affects how the layers stack. In the monoclinic Kröhnkite structure, the layers are related by a rotation and then a translation, whereas in the triclinic Fairfieldite structure, the layers are linked through translation. The structures also differ in their sodium site connectivity; in the monoclinic structure the sodium sites are connected through a mixture of corner and edge sharing, while in the triclinic structure, the sites are all edge sharing.

Although previous literature has focused purely on the identification and characterization of these endmember systems, research on solid solutions based on combinations of both sulfate (SO_4^{2-}) and selenate (SeO_4^{2-}) have been lacking. In particular, it is of interest to understand why there is a structural change from Kröhnkite to Fairfieldite for $Na_2M(XO_4)_2 \cdot 2H_2O$ (M=Co, Mn, Cu; X=S, Se) on changing from sulfate to selenate, and to determine at what substitution level does this structural change occur.

Another tetrahedral group, which is isovalent with SO_4^{2-} is fluorophosphate, PO_3F^{2-}. Fluorophosphate (PO_3F^{2-}) and mixed fluorophosphate/phosphate systems ($PO_{4-x}F_x^{2-}$) were first prepared and described over 80 years ago [19] . However despite a number of

applications, particularly in dental care, little of their potential to provide new materials has been explored until recently. In this respect, Weller and co-workers have recently exploited the fluorophosphate unit to access a range of new chemical systems [20–22]. An important aspect of the PO_3F^{2-} unit is that it possesses an electric dipole moment, and in reported structures there appears to be order in the relative orientations of the PO_3F^{2-} units to cancel these dipoles. Moreover, the structures of most PO_3F^{2-} containing phases, which possess waters of crystallisation, indicate that the F does not readily participate in H-bonding. Therefore in hydrated phases it does not necessarily provide a structural analogue to sulfate – opening up many more structural possibilities. Thus in this work, in addition to selenate doping, the influence of fluorophosphate doping has been examined on the structures of these $Na_2M(SO_4)_2 \cdot 2H_2O$ (M=Fe, Co, Mn, Ni, Cu) materials.

2. Experimental

The sodium transition metal sulfate hydrates were synthesized via a simple dissolution/evaporation route. Stoichiometric amounts of $MSO_4 \cdot yH_2O$ (Sigma Aldrich, 99%)(where M = Mn, Fe, Co, Ni and Cu, y = 1 for Fe and Mn, 5 for Cu, 6 for Ni and 7 for Co) and sodium sulfate (Sigma Aldrich, 99%) were dissolved in water. For the Fe containing samples, approximately 50mg of ascorbic acid was added to the solutions in order to prevent oxidation of Fe^{2+}. The solutions were stirred for at least 30 minutes at 60°C. The samples were then placed in an oven and dried at 60-110°C for Mn, Fe, Co and Cu samples and 130°C for Ni (The slightly higher temperature of 130°C was required for the Ni samples in order to obtain a single phase sample of the dihydrate; sample treatment <130°C yielded a mixture of the dihydrate and tetrahydrate phases).

$Na_2M(SO_4)_{2-x}(PO_3F)_x \cdot 2H_2O$ and $Na_2M(SO_4)_{2-x}(SeO_4)_x \cdot 2H_2O$ (where M = Mn, Fe, Co, Ni and Cu) were synthesized using the same solution method, where partial substitution of sodium sulfate by either sodium fluorophosphate or sodium selenate was performed. Given that Na_2SeO_4 and Na_2PO_3F were used as the source of selenate and fluorophosphate respectively, the maximum level of doping examined was 50% substitution (i.e. x=1).

$$MSO_4.yH_2O + 1\text{-}x\ Na_2SO_4 + x\ Na_2SeO_4/Na_2PO_3F \longrightarrow$$

$$Na_2M(SO_4)_{2-x}(SeO_4)/(PO_3F)_x \cdot 2H_2O$$

This synthetic approach has been previously shown to be successful in the preparation of other mixed sulfate/selenate systems e.g. NASICON type $Na_xM(II)_xM(III)_{2-x}(SO_4)_{3-y}(SeO_4)_y$ (M(II) = divalent metal, M(III) = trivalent metal) [23].

Sample purity and unit cell parameters were determined from powder X-ray diffraction using a Bruker D2 phaser (Co Kα radiation) and a Bruker D8 (Cu Kα radiation) operating in reflection mode. Rietveld refinements were carried out using the GSAS suite of programs.[24],[25] The starting structural models used for these materials were based on the structures reported for $Na_2Mn(SO_4)_2 \cdot 2H_2O$ and $Na_2Co(SeO_4)_2 \cdot 2H_2O$[18]. The cell parameters and atomic coordinates were refined with the exception of the protons in the system. In cases where a biphasic mixture was obtained, multiphase refinements were attempted to ascertain the fraction of each of the phases present. Further characterisation of these systems was performed using Raman spectroscopy (Renishaw in Via Raman microscope equipped with a He-Ne 633 nm laser).

3. Results and discussion

X-ray diffraction data for $Na_2M(SO_4)_2 \cdot 2H_2O$ (M=Mn, Fe, Co, Ni, Cu)

For both the undoped sulfate samples and the selenate/fluorophosphate doped samples, the samples possessed the following colours: Light brown (Fe), Pale pink (Co), Pale green (Ni) and Pale blue (Cu).

Depending on the metal cation employed to form the framework, the X-ray diffraction patterns show that two possible structures are observed through the dissolution/evaporation method employed (Fig. 2). For Mn, Fe, Co and Cu, the $Na_2M(SO_4)_2 \cdot 2H_2O$ phase crystallizes in the expected monoclinic Kröhnkite structure. However, when the metal ion is nickel, i.e. $Na_2Ni(SO_4)_2 \cdot 2H_2O$, the material adopts the triclinic Fairfieldite structure. As noted in the introduction, the structures both form 3-dimensional networks composed of metal octahedra corner sharing with sulfate tetrahedra, with chains of $M(SO_4)_4(H_2O)_2$ along the c-axis and the space between these chains occupied by the sodium ions, with a key difference being in terms of the H bonding network that links the layers (Fig. 1). This network, and so changeover in structure, may be influenced by the size of the transition metal. In this respect it is interesting to note that the triclinic structure is only observed for the smallest transition metal ion (Ni) (\ionic radii (high spin) M^{II}: Mn 0.83 Å, Fe 0.78 Å, Co 0.745 Å, Ni 0.69 Å, 0.73 Å).[26]

X-ray diffraction data for $Na_2M(SO_4)_{2-x}(SeO_4)_x \cdot 2H_2O$ $^{-}$ (M = Mn, Fe, Co, Ni and Cu)

A list of successfully synthesized selenate doped materials and the lattice parameters for these phases can be found in Tables 1-4 (when a composition yielded a biphasic sample, a two phase refinement was attempted to quantify the amount of each phase present) (Rietveld refinement profile fits are given in supplementary information).

The resulting material obtained was found to be dependent on the metal ion selected and level of selenate substitution attempted. In the case of M=Mn, there was no change in structure, with all compositions in the range of x = 0.1-1.0 retaining the monoclinic structure. For M=Fe samples, the monoclinic structure is again preferred for low level selenate incorporation. However, for $0.5 \leq x < 0.75$, a bi-phasic (monoclinic and triclinic) mixture is observed. Increasing the selenate concentration further to $x \geq 0.75$ results in a single phase material with the triclinic structure (Fig. 3). For the Co analogue, similar results were observed, albeit with a lower level of selenate (x=0.5) required to form the pure triclinic phase. For M=Cu, the results were also similar to the Co based system with compositions with $x \geq 0.5$ being phase pure triclinic structure.

For M=Ni, for which the sulfate endmember phase already adopts the triclinic structure, substitution of the sulfate for selenate readily occurs even at low dopant levels leading to a complete solid solution for the range of samples investigated ($0 \leq x \leq 1$)(Fig. 4).

Cell parameter data for all solid solution series show that Vegard's law is obeyed across the series, with increasing cell parameters on increasing selenate content as expected, due to the larger size of selenate versus sulfate.

The change in structure from monoclinic to triclinic for M=Mn, Co, Fe is most likely related to changes in the strength/nature of H-bonding caused by the introduction of selenate, leading to changes in the relative stabilities between the two structures. In the prior section on the sulfate series, $Na_2M(SO_4)_2 \cdot 2H_2O$, it was noted that the triclinic structure was formed only for the smallest transition metal, Ni. Considering the selenate doping results, both Co and Cu, which are the next smallest ions (and have similar ionic radii to one another), display a changeover from monoclinic to triclinic at a similar selenate content. For M=Fe, which has a larger ionic radius, a higher selenate content is required, while no changeover was observed

for M=Mn (the largest divalent ion) for the selenate doping level examined in this report. Furthermore no changeover in structure was reported for the endmember selenate phase, $Na_2Mn(SO_4)_{2-x}(SeO_4)_x \cdot 2H_2O$ prepared in a previous study[18]. Thus it appears that doping the larger selenate in place of sulfate is improving the stability of the triclinic structure for the smaller transition metals.

X-ray diffraction data for $Na_2M(SO_4)_{2-x}(PO_3F)_x \cdot 2H_2O$ (M= Mn, Fe, Co, Ni and Cu)

For M=Co, Cu, similar to the results for selenate doping, the monoclinic structure is not retained when doped with fluorophosphate. Instead, the X-ray diffraction data indicate that there is a structural change to the triclinic (Fairfieldite) struture (Fig 5). In this case, however, the change in structure is observed even at the lowest level of PO_3F^{2-} doping (x=0.1) examined.

This change in structure is most likely a result of the effect of PO_3F^{2-} altering the relative stabilities of the two (monoclinic vs triclinic) structures, through the PO_3F^{2-} group disrupting the H-bonding network, since covalently bound fluorine is well known to rarely participate in intermolecular hydrogen bonding.[27],[28]. This disruption of the H-bonding network by the fluorophosphate could be associated with the the fluorine within the PO_3F^{2-} unit pointing towards the network, since two O atoms from the tetrahedra are involved in H-bonding for the monoclinic (Kröhnkite) structure, while only one O is involved for the triclinic (fairfieldite) structure, so the presence of PO_3F^{2-} may improve the relative stability of the latter. The cell parameters of the phases obtained after substitution (Tables 6 and 7) have been plotted against fluorophosphate concentration (Fig. 6). In the case of Co, very little change is observed in the cell volume after the phase has adopted the triclinic structure. The

Cu system, however, does show a small cell volume increase with increasing fluorophosphate concentration.

For the larger Fe^{2+} system, the PO_3F^{2-} doping was not sufficient to cause the monoclinic to triclinic structural change. Rather, in this case, low levels of fluorophosphate led to the peaks in the resultant diffraction pattern exhibiting a wide range of peak widths, with some peaks remaining sharp while others broadened with increasing fluorophosphate concentration (Fig 7.). This peak broadening suggests a degree of local disorder within the structure, although on initial inspection, a single axis does not appear to be greatly affected. Greater evaluation of the Bragg reflections show that planes which intersect the hydrogen bond network or cut the corners of the tetrahedra appear to be the most affected with increasing fluorophosphate content. Planes which bisect the octahedra or tetrahedra without cutting through the network appear to be the least affected. This suggests that fluorophosphate has successfully doped into the system and is disrupting the hydrogen bond network. This proposed disruption is also supported by the fact that only low levels ($x \leq 0.3$) of PO_3F^{2-} can be incorported into the structure. Efforts to increase the concentration above x = 0.3 leads to a mixture of the doped phase and starting materials, i.e. Na_2SO_4, Na_2PO_3F and $MSO_4 \cdot xH_2O$.

The possible incorporation of PO_3F^{2-} for M=Mn, Ni was also examined, but in these cases the doping strategy was unsuccessful. In the case of Ni, a slightly higher temperature is required to form the dihydrate compared to the other $Na_2M(SO_4)_2$ systems, and so this may have promoted the hydrolysis of the fluorophosphate dopant, leading to $NaNi(SO_4)F \cdot 2H_2O$ impurity phases. In the case of M=Mn, at the lower temperatures required for PO_3F doping, Mn forms the highly hydrated $Na_{12}Mn_7(SO_4)_{13} \cdot 15H_2O$ system. With increasing PO_3F doping, the intensity of the peaks due to this phase decreases until x = 0.3 where the sample becomes amorphous.

Raman data for $Na_2M(SO_4)_{2-x}(SeO_4)_x \cdot 2H_2O$ (M= Fe, Co, Ni and Cu)

On selenate doping, the Raman data for $Na_2M(SO_4)_{2-x}(SeO_4)_x \cdot 2H_2O$ (M= Fe, Co, Ni and Cu) show the appearance of a set of broad peaks in the region of 800-900 cm^{-1} which increase in intensity with selenate content (Fig. 8). These peaks can be assigned to the ν^1 and ν^3 modes of Se-O in SeO_4.[29] Of note also is the small shift to decreasing wavenumber of the peak due to the ν^1 S-O mode. This shift suggests that sulfate and selenate occupy the same site and the strain on the system is reflected in the weakening of the S-O bond with increasing selenate concentration.

Raman data for $Na_2M(SO_4)_{2-x}(PO_3F)_x \cdot 2H_2O$ (M= Fe, Co and Cu)

The data for the monoclinic and triclinic phases appear to be very similar with the main difference originating from bands which can be assigned to asymmetric modes. Both spectra show the ν^1 S-O symmetric stretch band associated with $(SO_4)^{2-}$. The sulfate tetrahedra in both structures behave as a bidentate ligand by bridging the metal octahedra along the c-axis. This bonding leads to a splitting of the observed Raman peaks due to a reduction in symmetry of the oxoanion tetrahedra.[30] For M=Fe, when comparing the data for the undoped material with compositions containing a low level of fluorophosphate, a very weak peak at ~1030cm^{-1} appears to grow in intensity (this band can be identified on the shoulder of the ν^1 S-O band). The slight growth in intensity of the peak may pertain to the vibrational mode which corresponds to the ν_2 symmetrical stretch of the PO_3 unit within the PO_3F^{2-} group (Fig. 9).[31–33] Additional vibrations in the region of 1100-1200cm^{-1} also suggest a reduction in symmetry of the oxoanion unit. For M=Co and Cu, the spectra resulting from the fluorophosphates doped materials matched that which was obtained for the undoped $Na_2Ni(SO_4)_2 \cdot 2H_2O$ material which naturally adopts the triclinic structure (Fig. 10). This confirms that both of these materials have adopted the triclinic structure, however, the PO_3 band from the PO_3F^{2-} group is now hidden by an asymmetric (SO_4) band. An important

consideration in these systems is assessing whether the PO_3F^{2-} unit has remained intact or has hydrolysed to form PO_4^{3-}. One indication would be the presence of impurity phases, such as observed for M=Ni, where fluorophosphate doping was not successful. In addition, the Raman data also suggests the presence of PO_3F^{2-} rather than PO_4^{3-} as there are no bands in the regions of ~970cm^{-1} or ~520cm^{-1} which could be attributed to the P-O ν^1 and ν^4 respectively, which would be expected for PO_4^{3-}.[34] Although there may be some ambiguity due to potential overlap with the position of the ν_1 S-O band, the band attributed to PO_4^{3-} would be expected to appear at a lower wavenumber with respect to this band. As there are no observed peaks in this region, it can be assumed the system contains PO_3F^{2-} rather than PO_4^{3-}.

4. Conclusions

This work has shown the flexibility of $Na_2M(SO_4)_2{\cdot}2H_2O$ systems towards isoelectronic dopants such as $(PO_3F)^{2-}$ and $(SeO_4)^{2-}$ and the unique effect on the structure when a range of substitution levels are attempted. In particular, it is interesting to note that only the low levels of PO_3F^{2-} or SeO_4^{2-} are required (especially for PO_3F^{2-}) to cause a change in structure from the monoclinic (Krohnkite) to the triclinic (fairfieldite) structure, highlighting the potential of such a doping strategy to manipulate the structures of transition metal containing sulfate systems.

Acknowledgements

We would like to thank the University of Birmingham and the Midlands Energy Consortium for funding (studentship for LLD).

References

[1] G. Rousse, J.M. Tarascon, Sulfate-Based Polyanionic Compounds for Li-Ion Batteries: Synthesis, Crystal Chemistry, and Electrochemistry Aspects, Chem. Mater. 26 (2014) 394–406. doi:10.1021/cm4022358.

[2] P. Barpanda, Sulfate Chemistry for High-Voltage Insertion Materials: Synthetic, Structural and Electrochemical Insights, Isr. J. Chem. 55 (2015) 537–557. doi:10.1002/ijch.201400157.

[3] C. Masquelier, L. Croguennec, Polyanionic (phosphates, silicates, sulfates) frameworks as electrode materials for rechargeable Li (or Na) batteries, Chem. Rev. 113 (2013) 6552–6591. doi:10.1021/cr3001862.

[4] G. Oyama, S. Nishimura, Y. Suzuki, M. Okubo, A. Yamada, Off-Stoichiometry in Alluaudite-Type Sodium Iron Sulfate Na 2+2 x Fe 2− x (SO 4) 3 as an Advanced Sodium Battery Cathode Material, ChemElectroChem. 2 (2015) 1019–1023. doi:10.1002/celc.201500036.

[5] M. Reynaud, G. Rousse, A.M. Abakumov, M.T. Sougrati, G. Van Tendeloo, J.-N. Chotard, et al., Design of new electrode materials for Li-ion and Na-ion batteries from the bloedite mineral Na2Mg(SO4)2·4H2O, J. Mater. Chem. A. 2 (2014) 2671–2680. doi:10.1039/c3ta13648e.

[6] P. Barpanda, G. Oyama, C.D. Ling, A. Yamada, Kröhnkite-type Na2Fe(SO4)2· 2H2O as a novel 3.25 v insertion compound for Na-ion batteries, Chem. Mater. 26 (2014) 1297–1299. doi:10.1021/cm4033226.

[7] P. Barpanda, G. Oyama, S.-I. Nishimura, S.-C. Chung, A. Yamada, A 3.8-V earth-abundant sodium battery electrode., Nat. Commun. 5 (2014) 4358. doi:10.1038/ncomms5358.

[8] E. Kendrick, J. Kendrick, A. Orera, P. Panchmatia, M.S. Islam, P.R. Slater, Novel aspects of the conduction mechanisms of electrolytes containing tetrahedral moieties, Fuel Cells. 11 (2011) 38–43. doi:10.1002/fuce.201000044.

[9] A. Orera, P.R. Slater, New Chemical Systems for Solid Oxide Fuel Cells †, Chem. Mater. 22 (2010) 675–690. doi:10.1021/cm902687z.

[10] N. Mahato, A. Banerjee, A. Gupta, S. Omar, K. Balani, Progress in material selection for solid oxide fuel cell technology: A review, Prog. Mater. Sci. 72 (2015) 141–337. doi:10.1016/j.pmatsci.2015.01.001.

[11] S.B. Adler, Factors governing oxygen reduction in solid oxide fuel cell cathodes, Chem. Rev. 104 (2004) 4791–4843. doi:Doi 10.1021/Cr020724o.

[12] B.C. Steele, A. Heinzel, Materials for fuel-cell technologies., Nature. 414 (2001) 345–352. doi:10.1038/35104620.

[13] N.Q. Minh, Ceramic Fuel Cells, J. Am. Ceram. Soc. 76 (1993) 563–588. doi:10.1111/j.1151-2916.1993.tb03645.x.

[14] K.J. Lilley, U. Gbureck, a J. Wright, D.F. Farrar, J.E. Barralet, Cement from

nanocrystalline hydroxyapatite: Effect of calcium phosphate ratio, J. Mater. Sci. Mater. Med. 16 (2005) 1185–1190. doi:10.1007/s10856-005-4727-2.

[15] J.E. Barralet, L. Grover, T. Gaunt, a. J. Wright, I.R. Gibson, Preparation of macroporous calcium phosphate cement tissue engineering scaffold, Biomaterials. 23 (2002) 3063–3072. doi:10.1016/S0142-9612(01)00401-X.

[16] G. Buxbaum, G. Pfaff, Industrial Inorganic Pigments, Wiley-VCH, Mörlenbach, 2005.

[17] F.C. Hawthorne, R.B. Ferguson, Refinement of crystal-structure of Krohnkite, Acta Crystallogr. Sect. B-Structural Sci. 31 (1975) 1753–1755. doi:10.1107/S0567740875006048.

[18] M. Wildner, D. Stoilova, Crystal structures and crystal chemical relationships of krohnkite- and collinsite-type compounds Na2Me2+(XO4)(2)center dot 2 H2O (X = S, Me = Mn, Cd; and X = Se, Me = Mn, Co, Ni, Zn, Cd) and K2Co(SeO4)(2)center dot 2 H2O, 218 (2003) 201–209.

[19] W. Lange, Über die Vergleichbarkeit der Fluorsulfonate mit den Perchloraten in chemischer und krystallographischer Beziehung und über ein Fluorphosphat, Berichte Der Dtsch. Chem. Gesellschaft (A B Ser. 60 (1927) 962–970. doi:10.1002/cber.19270600422.

[20] K.L. Marshall, M.T. Weller, Synthesis of Titanium Fluorophosphates and Fluorosulfates from Hexafluorotitanic Acid, Zeitschrift Für Anorg. Und Allg. Chemie. 640 (2014) 2766–2770. doi:10.1002/zaac.201400362.

[21] E.R. Williams, K. Marshall, M.T. Weller, Copper(ii) chlorofluorophosphate: a new layered square-net for intercalating amines, CrystEngComm. 17 (2015) 160–164. doi:10.1039/C4CE01126K.

[22] A.C. Keates, J.A. Armstrong, M.T. Weller, Iron fluorophosphates, Dalt. Trans. 42 (2013) 10715–10724. doi:10.1039/C3DT50324K.

[23] P. Slater, C. Greaves, Synthesis and Conductivities of Sulfate/Selenate Phases Related to Nasicon: NaxM'(II)xM"(III)2-x(SO4)3-y(SeO4)y, J. Solid State Chem. 107 (1993) 12–18. http://linkinghub.elsevier.com/retrieve/pii/S0022459683713174.

[24] B.H. Toby, EXPGUI, a graphical user interface for GSAS, J. Appl. Crystallogr. 34 (2001) 210–213. doi:10.1107/S0021889801002242.

[25] A.C. Larson, R.B. Von Dreele, General Structure Analysis System (GSAS), Structure. 748 (2004) 86–748. doi:10.1103/PhysRevLett.101.107006.

[26] R.D. Shannon, Revised effective ionic radii and systematic studies of interatomic distances in halides and chalcogenides, Acta Crystallogr. Sect. A. 32 (1976) 751–767. doi:10.1107/S0567739476001551.

[27] H.A. Prescott, S.I. Troyanov, E. Kemnitz, The Synthesis and Crystal Structures of Two New Hydrated Sodium Monofluorophosphates: NaHPO3F·2.5 H2O (I) and Na2PO3F·10 H2O (II), J. Solid State Chem. 156 (2001) 415–421. doi:10.1006/jssc.2000.9016.

[28] J.D. Dunitz, R. Taylor, Organic Fluorine Hardly Ever Accepts Hydrogen Bonds, Chem. - A Eur. J. 3 (1997) 89–98. doi:10.1002/chem.19970030115.

[29] D. Stoilova, D. Marinova, M. Wildner, M. Georgiev, Comparative study on energetic distortions of SO4 2- ions matrix-isolated in compounds with krohnkite-type chains, K2Me(CrO4)2·2H2O and Na2Me(SeO4)2·2H2O (Me = Mg, Co, Ni, Zn, Cd), Solid State Sci. 11 (2009) 2044–2050. doi:10.1016/j.solidstatesciences.2009.09.011.

[30] R.L. Frost, Y. Xi, R. Scholz, Vibrational Spectroscopy of the Copper (II) Disodium Sulphate Dihydrate Mineral Kröhnkite Na2Cu(SO4)2 · 2H2O, Spectrosc. Lett. 46 (2013) 447–452. doi:10.1080/00387010.2012.753906.

[31] K.J. Koudelka L., Raman spectra and structure of fluorophosphate glasses of (1 - x)Ba(PO3) 2 - xLiRAIF 6, J. Non. Cryst. Solids. 85 (1986) 204–210.

[32] M. Weil, M. Puchberger, E.J. Baran, Preparation and characterization of dimercury(I) monofluorophosphate(V), Hg2PO3F: Crystal structure, thermal behavior, vibrational spectra, and solid-state 31P and 19F NMR spectra, Inorg. Chem. 43 (2004) 8330–8335. doi:10.1021/ic048741e.

[33] E.J. Baran, M. Weil, Vibrational spectra of the layered monofluorophosphate (V), $NH_4Ag_3(PO_3F)_2$, J. Raman Spectrosc. 40 (2009) 1698–1700. doi:10.1002/jrs.2461.

[34] R.L. Frost, S.J. Palmer, A vibrational spectroscopic study of the mixed anion mineral sanjuanite Al2(PO4)(SO4)(OH)·9H2O., Spectrochim. Acta. A. Mol. Biomol. Spectrosc. 79 (2011) 1210–1214. doi:10.1016/j.saa.2011.04.044.

Figure Captions

Figure 1. Crystal structures of $Na_2M(SO_4)_2 \cdot 2H_2O$ (M=Fe, Co) (above) and $Na_2Ni(SO_4)_2 \cdot 2H_2O$ (below) viewed down the a-axis. Brown/blue octahedra represent the transition metal ion (Fe/Co and Ni respectively). The green tetrahedra represent the sulfate oxyanion and the yellow spheres represent the sodium ions that reside within the layers. The dashed orange line shows the hydrogen bond network that aids in structure stabilization.

Figure 2. The diffraction patterns of monoclinic $Na_2Fe(SO_4)_2 \cdot 2H_2O$ and triclinic $Na_2Ni(SO_4)_2 \cdot 2H_2O$. The nickel sample contains a minor $NiSO_4 \cdot H_2O$ impurity (~3wt%). The impurity peaks are identified by black triangles. An unidentified peak has been labelled with a black square

Figure 3. Diffraction patterns of $Na_2Fe(SO_4)_{2-x}(SeO_4)_x \cdot 2H_2O$ where x = 0-1.0.

Figure 4. Diffraction patterns of end members $Na_2M(SO_4)(SeO_4) \cdot 2H_2O$ (where M = Fe, Co and Ni).

Figure 5. The diffraction patterns of $Na_2M(SO_4)_{2-x}(PO_3F)_x \cdot 2H_2O$ where M = Co and Cu and x = 0 - 0.25 for Co and 0-0.5 for Cu. Bragg positions for the monoclinic phase (Pink) and Triclinic (Teal) have been added to the plots to show that although some reflection positions appear similar in both structures, there are noticeable differences in the resultant diffraction patterns.

Figure 6. A plot of cell volume vs fluorophosphate concentration in $Na_2M(SO_4)_{2-x}(PO_3F)x \cdot 2H_2O$ where M = Cu and Co and x = 0.1-0.3.

Figure 7. (a). The X-ray diffraction patterns for $Na_2Fe(SO_4)_{2-x}(PO_3F)_x \cdot 2H_2O$; (b) Selected peaks from the diffraction pattern of $Na_2Fe(SO_4)_2 \cdot 2H_2O$ and $Na_2Fe(SO_4)_{1.9}(PO_3F)_{0.1} \cdot 2H_2O$. With PO_3F doping, peak broadening is observed for some peaks (e.g. (031), (12-1)), while others (e.g. (020)) are largely unaffected. The respective lattice planes are shown in the associated structural figures.

Figure 8. Raman data for hydrated $Na_2M(SO_4)(SeO_4) \cdot 2H_2O$ (M= Fe, Co, Ni and Cu (above) and $Na_2Ni(SO_4)_{2-x}(SeO_4)_x \cdot 2H_2O$ where x = 0-1(below)).

Figure 9. Raman data for $Na_2Fe(SO_4)_{2-x}(PO_3F)_x \cdot 2H_2O$. The weak peak at around 1030cm^{-1} grows slightly with increasing PO_3F concentration.

Figure 10. Raman data comparing the monoclinic and triclinic phases. The main difference in the data originates in the asymmetric S-O bands. Monoclinic phases have two weak bands in the 1100-1200cm^{-1} region where as the triclinic phases have three weak bands in the 1000-1200cm^{-1}. Co and Cu phases possess three bands in the 1000-1200 region suggesting successful formation of the triclinic phase.

Table 1. Cell parameters for $Na_2Fe(SO_4)_{2-x}(SeO_4)_x \cdot 2H_2O$

Note: M = Monoclinic and T = Triclinic with regards to the phase % of each formed.

Dopant level (x=)	a (Å)	b (Å)	c (Å)	α (°)	β (°)	γ (°)	Cell volume (Å^3)	W% (M:T)
0	5.7682(2)	12.9803(2)	5.4520(2)	90.0	105.960(2)	90.0	392.47(1)	(100:0)
0.1	5.7722(2)	12.9957(3)	5.4605(2)	90.0	105.946(3)	90.0	393.85(2)	(100:0)
0.25	5.7858(2)	13.0328(3)	5.4793(1)	90.0	105.928(2)	90.0	397.31(2)	(100:0)
0.5	5.7977(2)	13.0757(6)	5.5031(2)	90.0	105.887(2)	90.0	401.25(4)	(82:18)
	5.8798(9)	7.166(1)	5.5080(7)	98.50(2)	106.46(1)	108.50(1)	203.70(5)	
0.75	5.8407(3)	7.1799(4)	5.5252(3)	98.923(3)	106.188(3)	108.340(3)	203.59(2)	(0:100)
1.0	5.8560(4)	7.1921(4)	5.5424(3)	98.945(4)	106.266(4)	108.339 (3)	204.96(2)	(0:100)

Table 2. Cell parameters for $Na_2Co(SO_4)_{2-x}(SeO_4)_x \cdot 2H_2O$

Dopant level (x=)	a (Å)	b (Å)	c (Å)	α (°)	β (°)	γ (°)	Cell volume (Å^3)	W% (M:T)
0	5.7787(2)	12.8671(4)	5.3999(2)	90.0	105.862(2)	90.0	386.23(2)	(100:0)
0.1	5.770(3)	12.879(1)	5.402(9)	90.0	106.1(1)	90.0	385.7(6)	(33:67)
	5.7949(6)	7.0503(6)	5.4024(4)	98.881(8)	106.006(7)	108.580(7)	193.87(3)	
0.25	5.7733(8)	12.9043(7)	5.426(1)	90.0	105.85(1)	90.0	388.86(8)	(36:64)
	5.8033(5)	7.0647(5)	5.4108(5)	98.934(8)	105.969(7)	108.553(6)	194.88(2)	

0.5	5.8237(4)	7.0878(5)	5.4359(3)	98.933(5)	106.058(4)	108.602(3)	196.92(3)	(0:100)
0.75	5.8409(3)	7.1093(4)	5.4592(3)	98.970(4)	106.123(3)	108.553(3)	198.89(2)	(0:100)
1.0	5.8567(2)	7.1273(1)	5.4760(2)	98.953(2)	106.173(2)	108.561(4)	200.486(6)	(0:100)

Table 3. Cell parameters for $Na_2Ni(SO_4)_{2-x}(SeO_4)_x \cdot 2H_2O$

Dopant level (x=)	a (Å)	b (Å)	c (Å)	α (°)	β (°)	γ (°)	Cell vol. (Å^3)
0	5.7810(3)	7.0052(4)	5.3388(2)	99.096(4)	105.551(3)	108.609(3)	190.25(2)
0.1	5.7883(4)	7.0152(5)	5.3490(3)	99.143(6)	105.533(3)	108.587(3)	191.13(2)
0.25	5.7944(4)	7.0267(5)	5.3601(3)	99.159(6)	105.590(4)	108.594(3)	191.94(3)
0.5	5.8118(7)	7.0547(9)	5.3865(5)	99.22(1)	105.679(6)	108.570(5)	194.08(4)
0.75	5.8239(6)	7.0702(7)	5.4055(4)	99.238(9)	105.786(5)	108.558(4)	195.46(3)
1.0	5.8389(7)	7.0943(8)	5.4307(5)	99.22(1)	105.919(7)	108.579(5)	197.35(4)

Table 4. Cell parameters for $Na_2Cu(SO_4)_{2-x}(SeO_4)_x \cdot 2H_2O$

Dopant level (x=)	a (Å)	b (Å)	c (Å)	α (°)	β (°)	γ (°)	Cell vol. (Å^3)	W% (M:T)
0	5.8002(3)	12.6493(8)	5.5102(3)	90.0	108.442(2)	90.0	383.51(6)	(100:0)
0.1	5.8216(5)	12.699(1)	5.5310(5)	90.0	108.423(4)	90.0	387.93(7)	(58:42)
	5.8181(6)	6.9625(6)	5.5177(5)	101.307(7)	108.421(5)	106.129(5)	193.58(3)	
0.2	5.8196(4)	12.670(1)	5.5342(4)	90.0	108.420(5)	90.0	388.06(6)	(45:55)
	5.8216(4)	6.9693(5)	5.5227(3)	101.305(5)	108.446(4)	106.128(4)	194.03(2)	
0.3	5.8266(5)	12.714(1)	5.5422(5)	90.0	108.413(5)	90.0	389.54(6)	(38:62)
	5.8286(4)	6.9772(4)	5.5309(3)	101.307(4)	108.438(4)	106.130(3)	194.78(2)	
0.5	5.840(1)	12.746(3)	5.550(2)	90.0	108.4(2)	90.0	391.9(1)	(19:81)

	5.8447(4)	6.9948(4)	5.5506(3)	101.315(4)	108.462(3)	106.123(3)	196.47(3)	
0.75	5.8622(2)	7.0148(3)	5.5732(2)	101.325(3)	108.492(2)	106.126(2)	198.36(2)	(0:100)
1.0	5.8776(3)	7.0358(3)	5.5936(2)	101.345(3)	108.504(2)	106.118(2)	200.17(2)	(0:100)

Table 5. Cell parameters for $Na_2Fe(SO_4)_{2-X}(PO_3F)_x \cdot 2H_2O$

Dopant level (x=)	a (Å)	b (Å)	c (Å)	α (°)	β (°)	γ (°)	Cell volume ($Å^3$)
0	5.7682(2)	12.9803(2)	5.4520(2)	90.0	105.960(2)	90.0	392.47(1)
0.05	5.7618(9)	12.978(2)	5.4474(5)	90.0	105.947(7)	90.0	391.7(1)

Table 6. Cell parameters for $Na_2Co(SO_4)_{2-X}(PO_3F)_x \cdot 2H_2O$

Dopant level (x=)	a (Å)	b (Å)	c (Å)	α (°)	β (°)	γ (°)	Cell volume ($Å^3$)
0	5.7787(2)	12.8671(4)	5.3999(2)	90.0	105.862(2)	90.0	386.23(2)
0.1	5.7901(3)	7.0465(3)	5.3937(3)	98.891(4)	106.025(3)	108.604(3)	193.22(2)
0.15	5.7892(4)	7.0512(5)	5.3926(3)	98.961(5)	105.970(4)	108.574(3)	193.32(3)
0.2	5.7898(3)	7.0522(3)	5.3913(2)	98.967(4)	105.972(3)	108.584(3)	193.30(2)
0.25	5.7901(4)	7.0544(5)	5.3909(3)	99.031(6)	105.890(5)	108.654(4)	193.30(3)

Table 7. Cell parameters for $Na_2Cu(SO_4)_{2-X}(PO_3F)_x \cdot 2H_2O$

Dopant level (x=)	a (Å)	b (Å)	c (Å)	α (°)	β (°)	γ (°)	Cell volume ($Å^3$)
0	5.8002(3)	12.6493(8)	5.5102(3)	90.0	108.442(2)	90.0	383.51(6)
0.1	5.8059(3)	6.9484(3)	5.5012(2)	101.364(3)	108.410(2)	106.110(2)	192.18(2)

0.2	5.8100(4)	6.9510(4)	5.5029(3)	101.390(4)	108.404(3)	106.113(3)	192.42(3)
0.3	5.8149(3)	6.9572(3)	5.5081(2)	101.409(3)	108.392(2)	106.092(2)	192.97(2)

Figure 1. Crystal structures of $Na_2Fe/Co(SO_4)_2 \cdot 2H_2O$ (above) and $Na_2Ni(SO_4)_2 \cdot 2H_2O$ (below) viewed down the a-axis. Brown/blue octahedra represent the transition metal ion (Fe/Co and Ni respectively). The green tetrahedra represent the sulfate oxyanion and the yellow spheres represent the sodium ions that reside within the layers. The dashed orange line shows the hydrogen bond network that aids in structure stabilization.

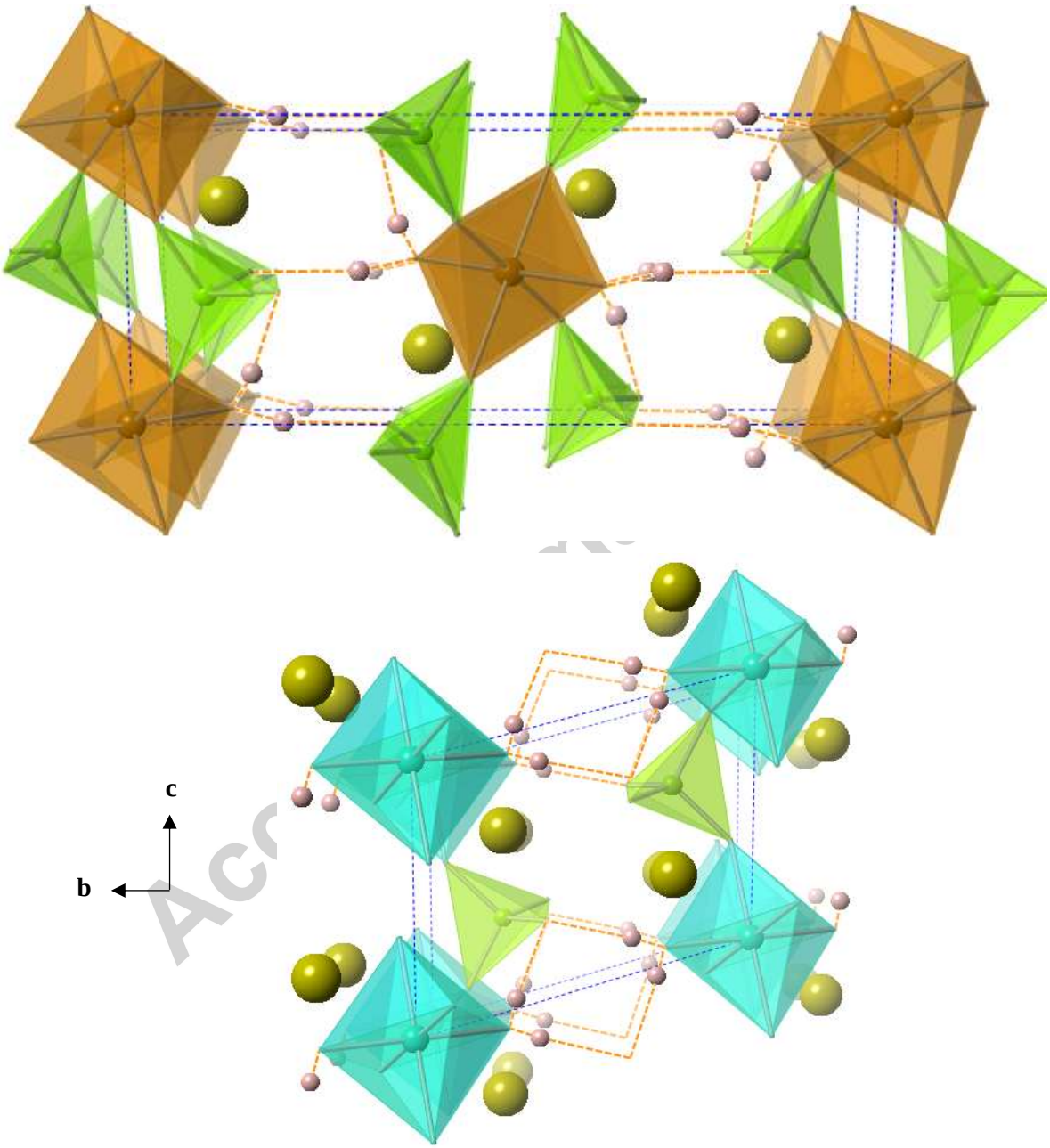

Figure 2. The diffraction patterns of monoclinic $Na_2Fe(SO_4)_2 \cdot 2H_2O$ and triclinic $Na_2Ni(SO_4)_2 \cdot 2H_2O$. The nickel sample contains a minor $NiSO_4 \cdot H_2O$ impurity (~3wt%). The impurity peaks are identified by black triangles. An unidentified peak has been labelled with a black square.

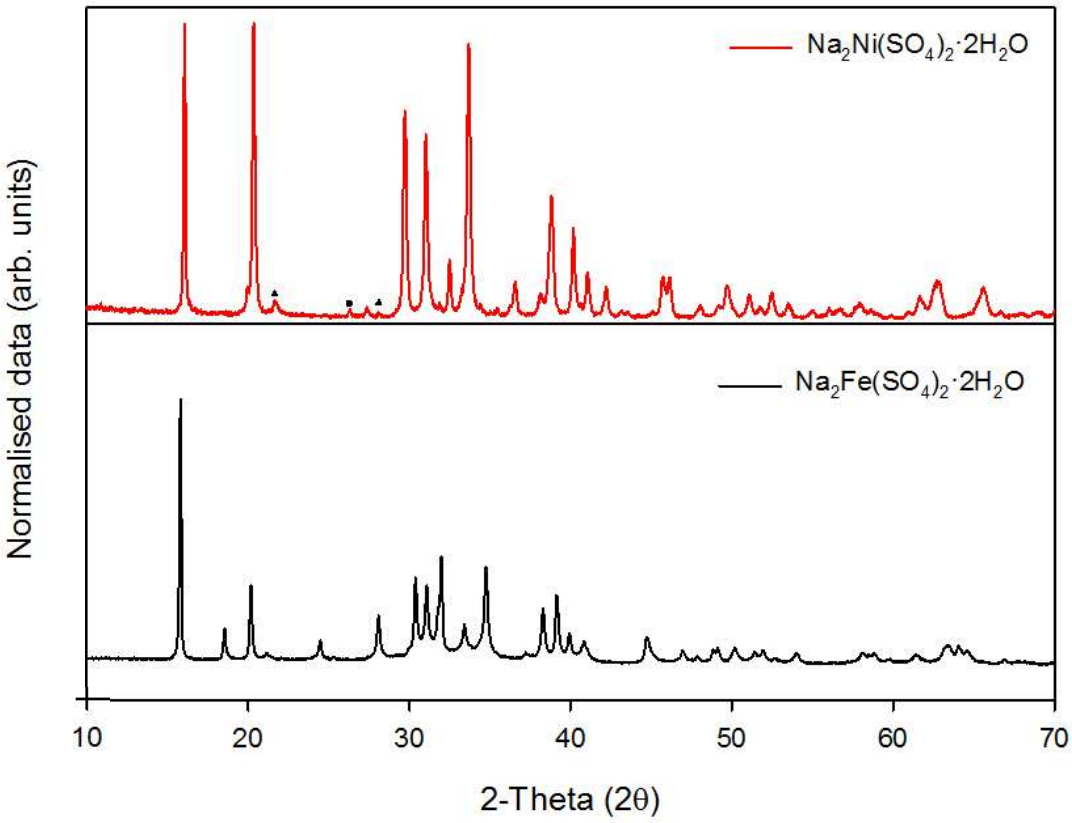

Figure 3. Diffraction patterns of $Na_2Fe(SO_4)_{2-x}(SeO_4)_x \cdot 2H_2O$ where x = 0-1.0.

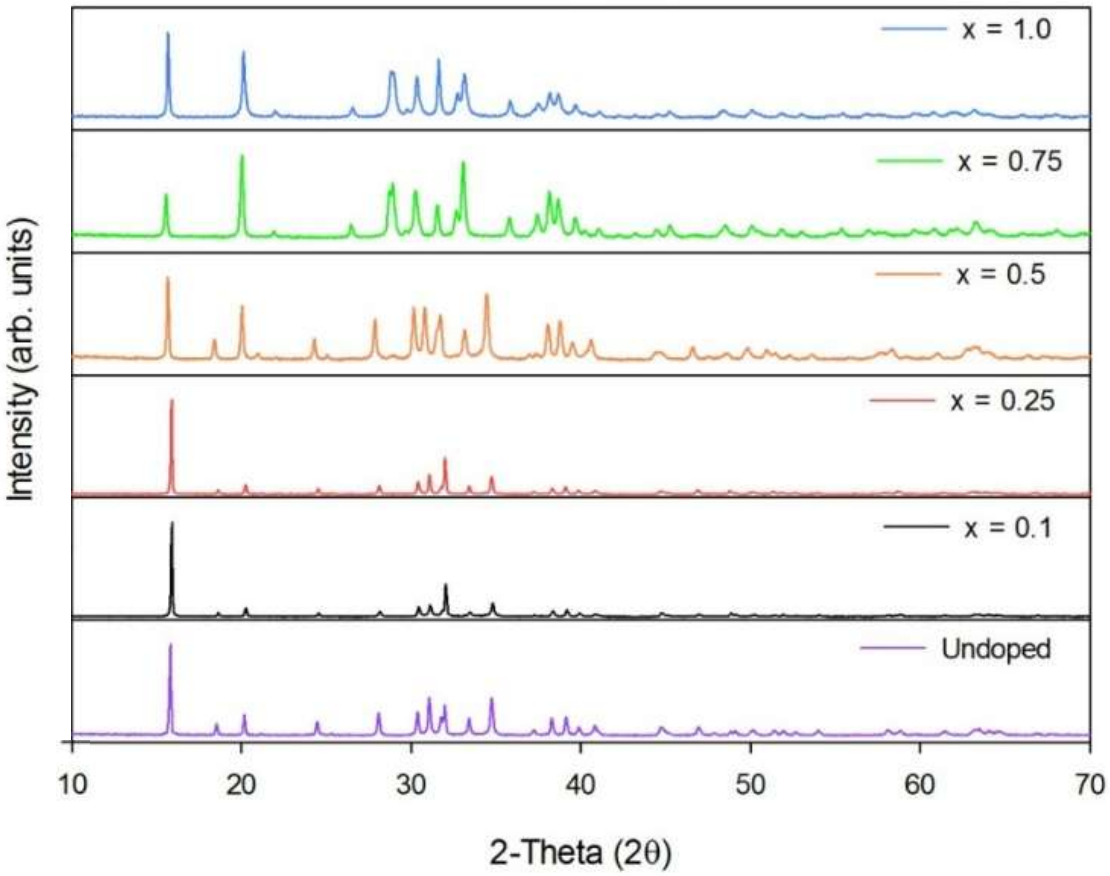

Figure 4. Diffraction patterns of end members $Na_2M(SO_4)(SeO_4)\cdot 2H_2O$ (where M = Fe, Co and Ni).

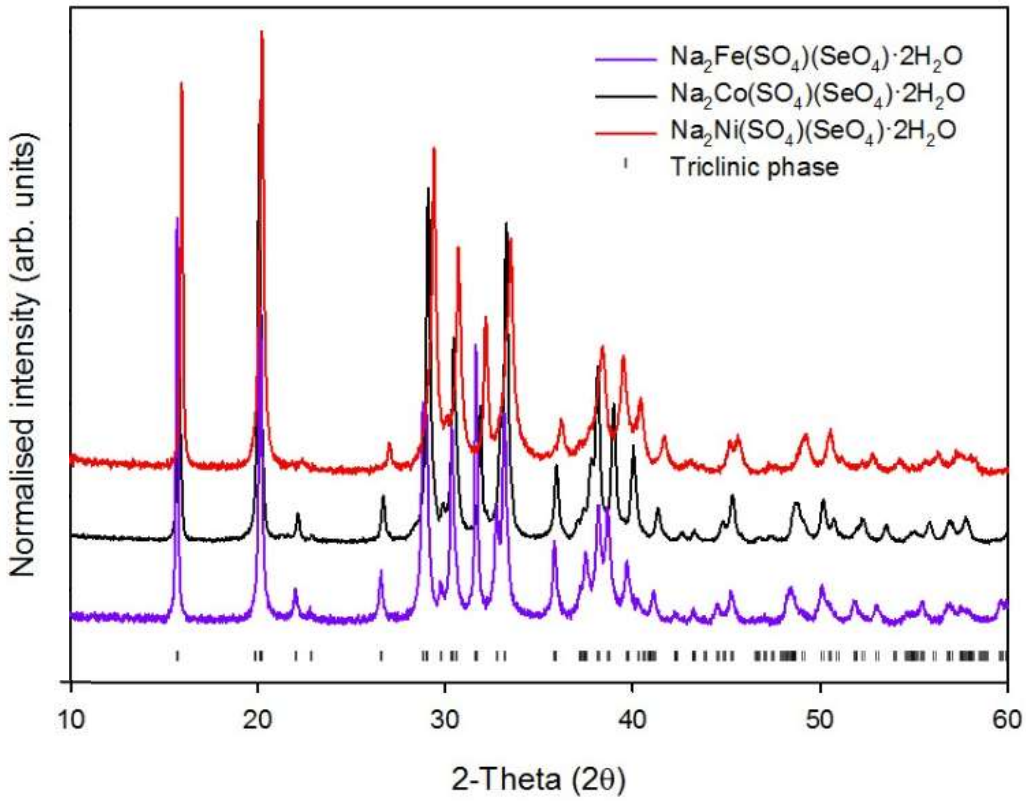

Figure 5. The diffraction patterns of $Na_2M(SO_4)_{2-x}(PO_3F)_x \cdot 2H_2O$ where M = Co and Cu and x = 0 - 0.25 for Co and 0-0.5 for Cu. Bragg positions for the monoclinic phase (Pink) and Triclinic (blue) have been added to the plots to show that although some reflection positions appear similar in both structures, there are noticeable differences in the resultant diffraction patterns.

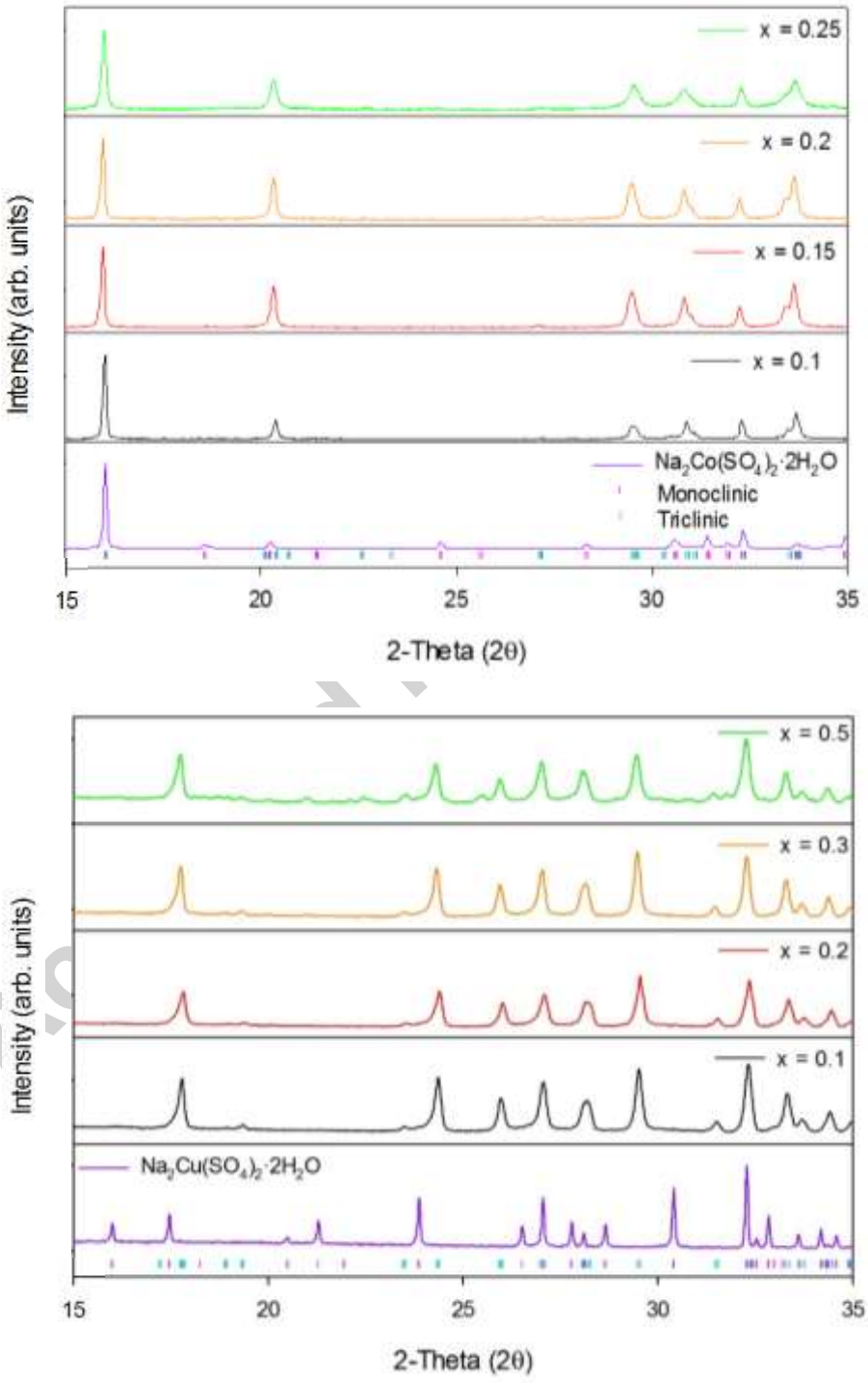

Figure 6. A plot of cell volume vs fluorophosphate concentration in $Na_2M(SO_4)_{2-x}(PO_3F)x \cdot 2H_2O$ where M = Cu and Co and x = 0.1-0.3.

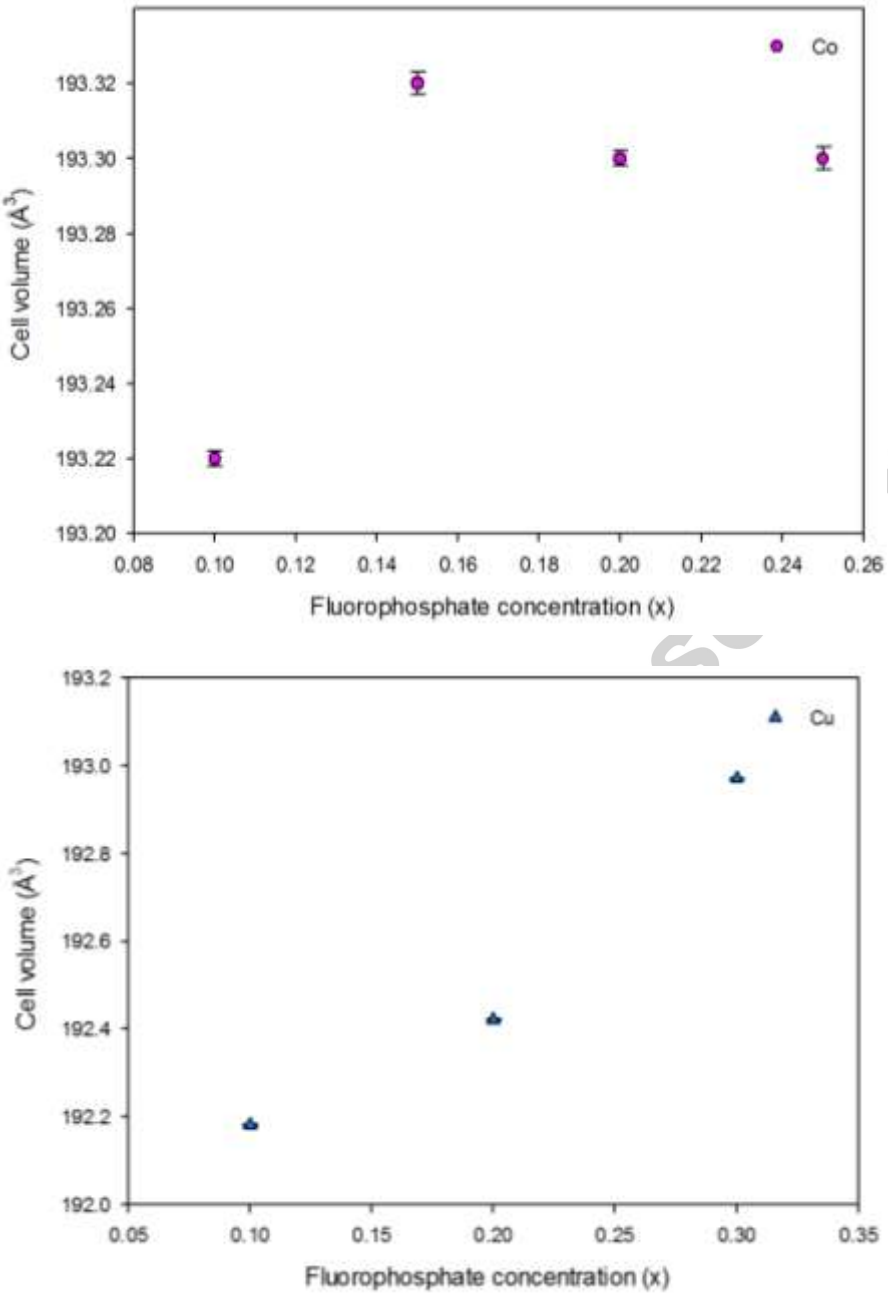

Figure 7(a). The X-ray diffraction patterns for $Na_2Fe(SO_4)_{2-x}(PO_3F)_x \cdot 2H_2O$

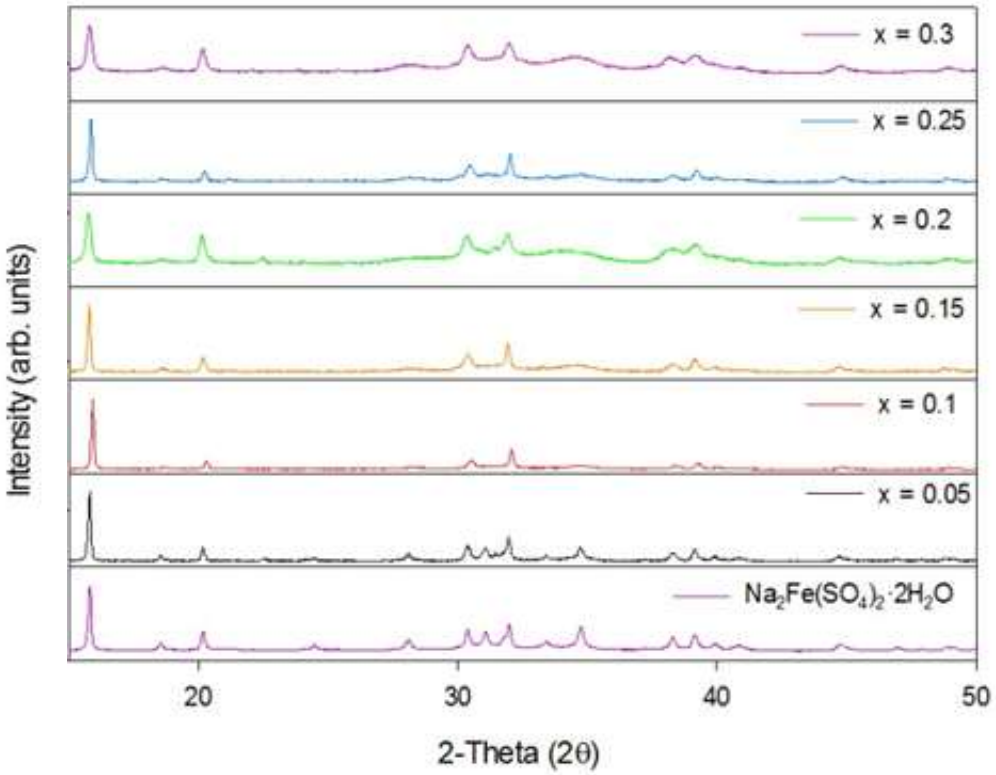

Figure 7(b) Selected peaks from the diffraction pattern of $Na_2Fe(SO_4)_2 \cdot 2H_2O$ and $Na_2Fe(SO_4)_{1.9}(PO_3F)_{0.1} \cdot 2H_2O$. With PO_3F doping, peak broadening is observed for some peaks (e.g. (031), (12-1)), while others (e.g. (020)) are largely unaffected. The respective lattice planes are shown in the associated structural figures.

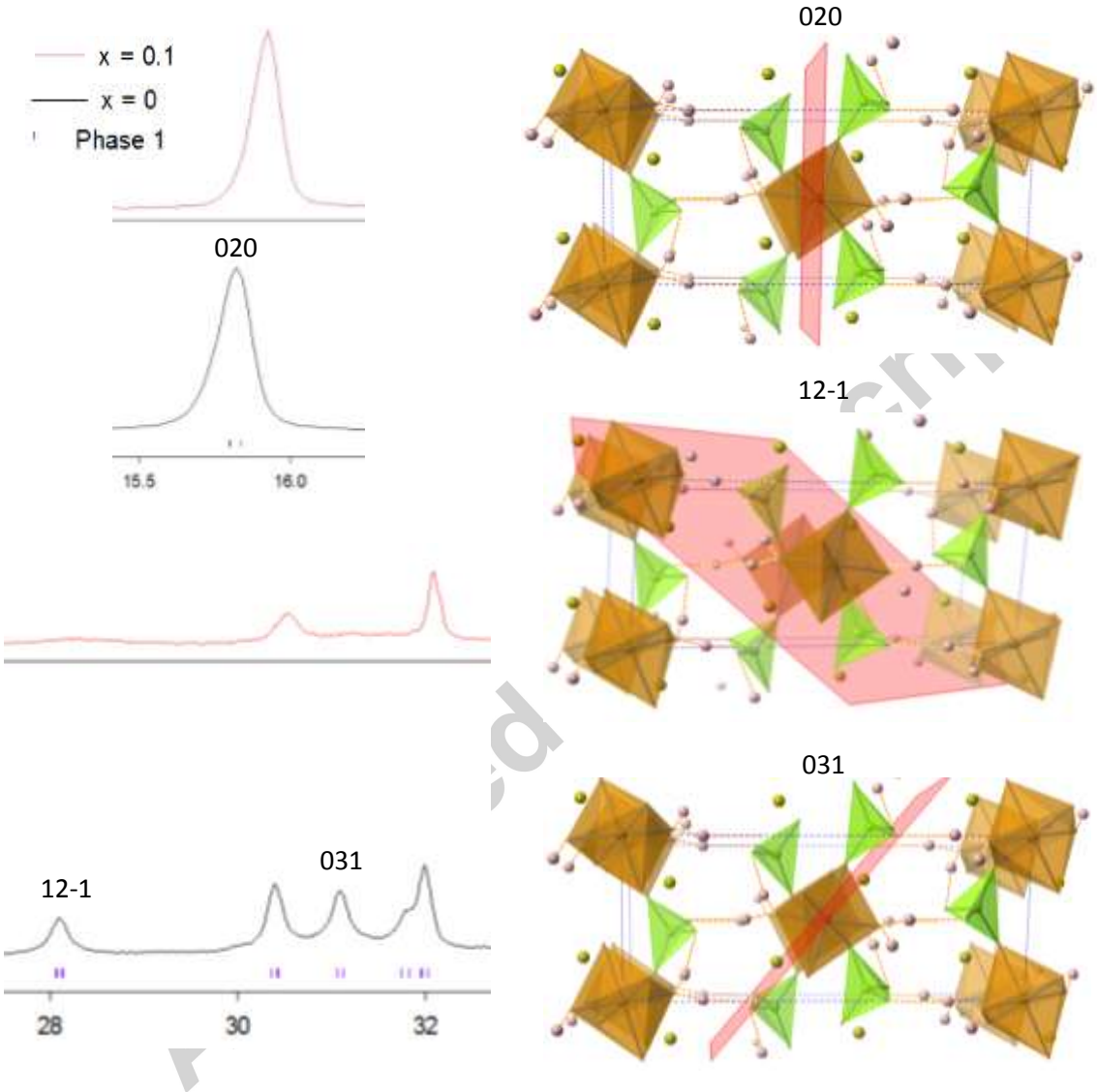

Figure 8. Raman data for hydrated $Na_2M(SO_4)(SeO_4)\cdot 2H_2O$ (M= Fe, Co, Ni and Cu (above) and $Na_2Ni(SO_4)_{2-x}(SeO_4)_x\cdot 2H_2O$ where x = 0-1(below)).

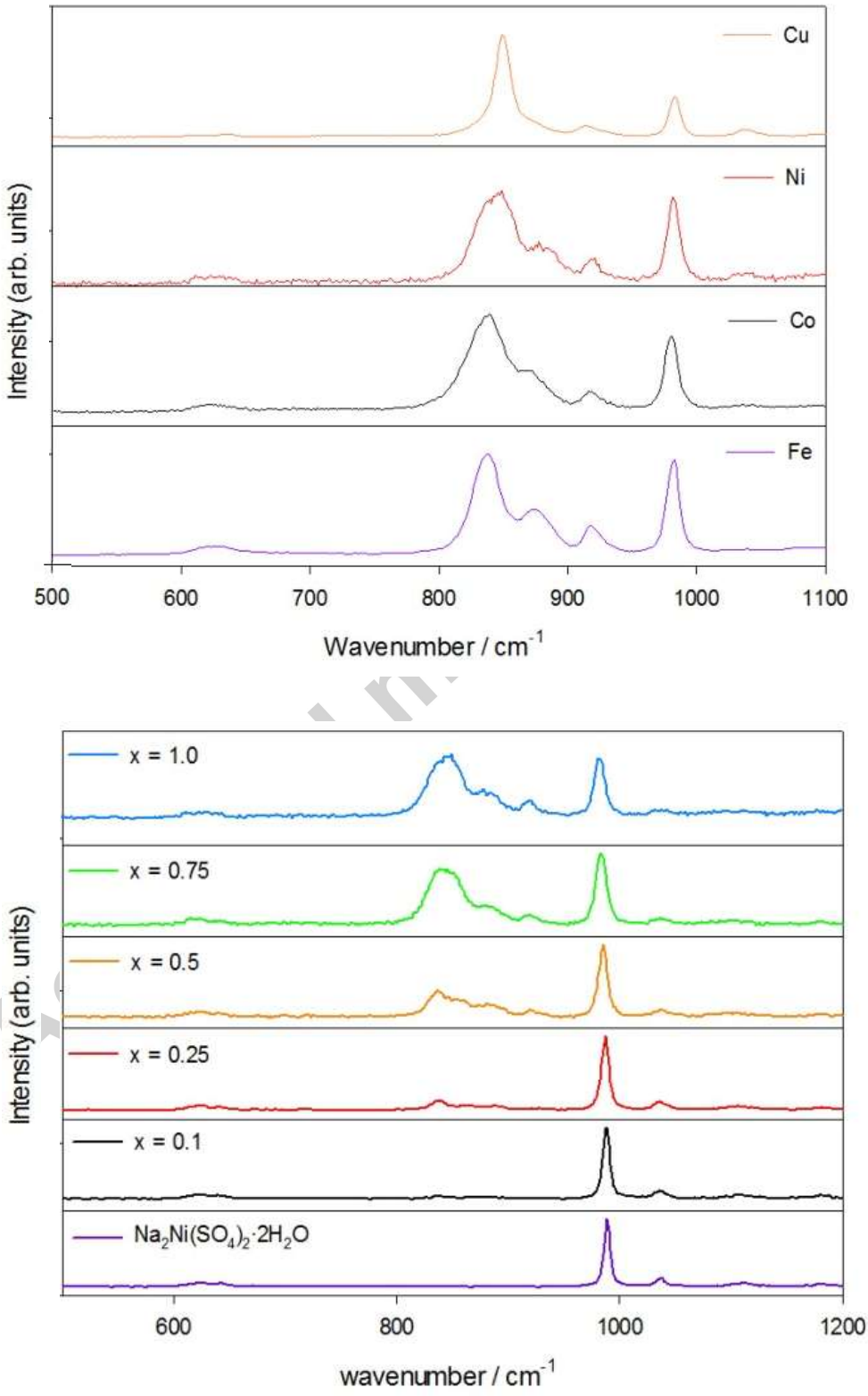

Figure 9. Raman data for $Na_2Fe(SO_4)_{2-x}(PO_3F)_x \cdot 2H_2O$. The very weak peak at around 1030cm^{-1} grows slightly with increasing PO_3F concentration.

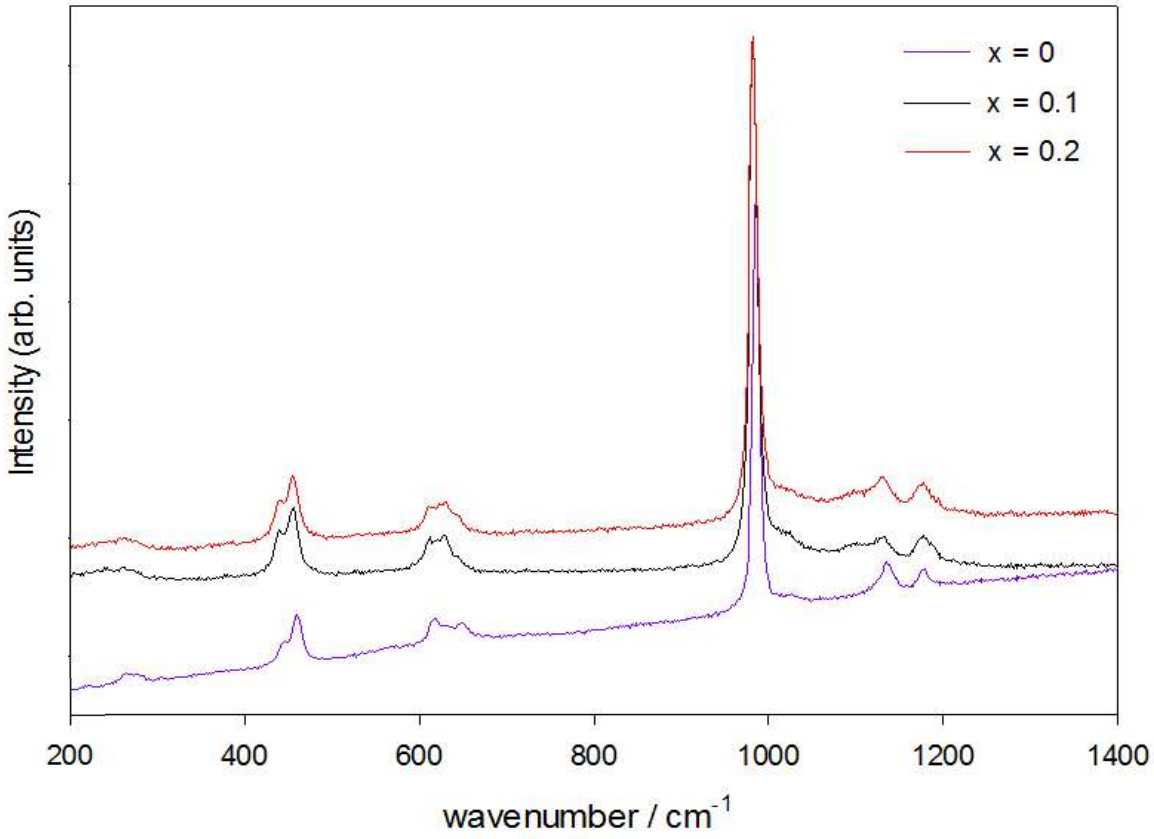

Figure 10. Raman data comparing the monoclinic and triclinic phases. The main difference in the data originates in the asymmetric S-O bands. Monoclinic phases have two weak bands in the 1100-1200cm^{-1} region where as the triclinic phases have three weak bands in the 1000-1200cm^{-1}. Co and Cu phases possess three bands in the 1000-1200 region suggesting successful formation of the triclinic phase.

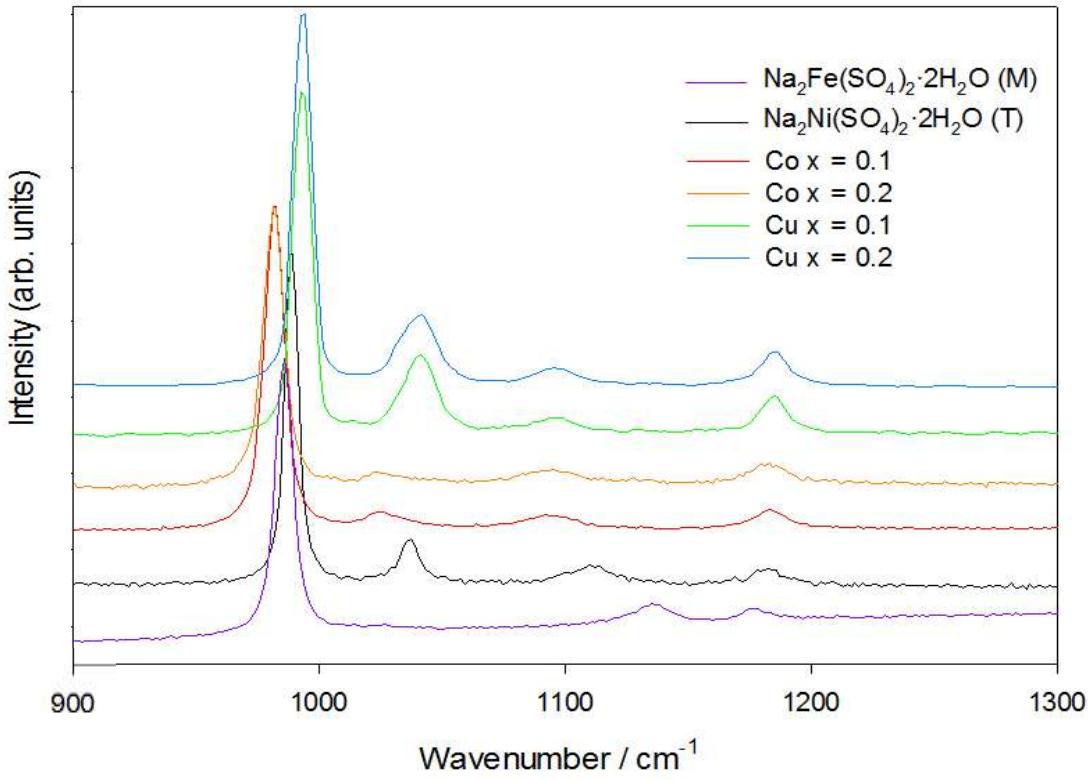

Highlights

- The successful synthesis of $Na_2M(SO_4)_2 \cdot 2H_2O$ (M=transition metal) phases doped with selenate and fluorophosphate.
- A change in structure is observed on selenate doping for M=Fe, Co, Cu.
- This change in structure is also observed on fluorophosphate doping for M=Co, Cu, with very low fluorophosphate levels (5mol% doping) causing the structural change.

- The work highlights how isovalent doping can be exploited to alter the structures of $Na_2M(SO_4)_2 \cdot 2H_2O$ systems.

Graphical abstract

Partial substitution of sulfate in $Na_2M(SO_4)_2.2H_2O$ (M=Co, Cu) by selenate or fluorophosphate leads to a structural change from the monoclinic Kröhnkite to the triclinic Fairfieldite structure.

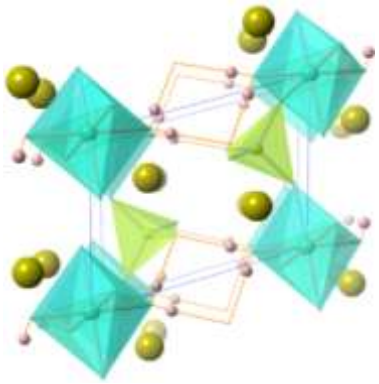

Partial substitution of sulfate in $Na_2M(SO_4)_2.2H_2O$ (M=Co, Cu) by selenate or fluorophosphate leads to a structural change from the monoclinic Kröhnkite to the triclinic Fairfieldite structure.